J|A|C|S COMMUNICATIONS

Published on Web 04/26/2010

High Proton Conductivity in Prussian Blue Analogues and the Interference Effect by Magnetic Ordering

Shin-ichi Ohkoshi,* Kosuke Nakagawa, Keisuke Tomono, Kenta Imoto, Yoshihide Tsunobuchi, and Hiroko Tokoro

Department of Chemistry, School of Science, The University of Tokyo, 7-3-1 Hongo, Bunkyo-ku, Tokyo 113-0033, Japan

Received January 15, 2010; E-mail: ohkoshi@chem.s.u-tokyo.ac.jp

Various interesting magnetic functionalities have been reported with Prussian blue analogues,[1] such as high magnetic ordering temperatures,[2] photomagnetism,[3] and chemically sensitive magnetism.[4] In addition, new functions have been recently studied on Prussian blue analogues,[5] including pressure-induced CN flip, zero thermal expansion, and hydrogen storage. Prussian blue analogues have two types of cubic crystal structures. One of them is $Fm\bar{3}m$ in $M_A^{II}[M_B^{III}(CN)_6]_{2/3}\cdot zH_2O$, where M_A and M_B are transition-metal ions. The other one is $F\bar{4}3m$ in $A^IM_A^{II}[M_B^{III}(CN)_6]$, in which the alkali ion A alternatively occupies in the interstitial sites. $M_A[M_B(CN)_6]_{2/3}\cdot zH_2O$ has vacancies of $[M_B(CN)_6]$ and ligand water molecules coordinated to the M_A ions, and zeolitic water molecules exist in the vacancy sites. Herein we report high proton conductivities (σ) of 1.2×10^{-3} S cm^{-1} for $Co[Cr(CN)_6]_{2/3}\cdot zH_2O$ (**1**) and 1.6×10^{-3} S cm^{-1} for $V[Cr(CN)_6]_{2/3}\cdot zH_2O$ (**2**) at room temperature. Additionally, **2** displays an interference effect between ionic conduction and magnetic ordering below the Curie temperature (T_C). This is the first observation of an interference effect between ionic conductivity and magnetic ordering.

1 was prepared using our previously reported procedure.[4a] **1** was a pink powder with a formula of $Co^{II}[Cr^{III}(CN)_6]_{2/3}\cdot 4.8H_2O$ (Calcd: Co, 20.8; Cr, 12.2; C, 16.9; N, 19.7%. Found: Co, 20.7; Cr, 12.2; C, 16.8; N, 19.8%.). The X-ray diffraction (XRD) pattern of **1** showed a face-centered cubic (fcc) crystal structure with a lattice constant of 10.560 Å. The CN stretching frequency in the IR spectrum was 2169 cm^{-1}. **2** was prepared using the modified procedure reported in Verdaguer's paper.[2f] **2** was synthesized by adding a mixed aqueous solution of $VSO_4\cdot 6H_2O$ (1.5 mL, 210 mM) and $VOSO_4\cdot 6H_2O$ (1.5 mL, 10 mM) to an aqueous solution of $K_3[Cr(CN)_6]$ (3 mL, 67 mM) at room temperature under an argon atmosphere. The solution was stirred for 1 min, and then the dark-purple precipitate was filtered off and washed with water. Elemental analyses confirmed that the formula was $V^{II}[Cr^{III}(CN)_6]_{2/3}\cdot 4.2H_2O$ (Calcd: V, 19.2; Cr, 13.0; C, 18.1; N, 21.1%. Found: V, 19.5; Cr, 12.9; C, 17.9; N, 21.0%.). The XRD pattern of **2** showed broad peaks due to the fcc structure (Figure S1 in the Supporting Information). The CN stretching frequency in the IR spectrum was 2110 cm^{-1}.

Conductivity measurements were carried out with an Agilent 4294A precision impedance analyzer using a quasi-four-probe method in the frequency range from 40 to 110 MHz. For each measurement, the powdered sample was compressed into a diameter of 7 mm and thickness of 1 mm using a sample holder with nickel-coated iron electrodes. The humidity of the sample holder for each measurement was tuned using dry N_2 that had been passed through water or a saturated aqueous solution of NaBr.

Figure 1a shows the real part (Z') and imaginary part (Z'') of the complex-plane impedance data for **1**. Cole−Cole circular arc fitting gave a σ value of 1.2×10^{-3} S cm^{-1} at 293 K at 100% relative humidity (RH). As the temperature was increased, the σ value increased from 1.2×10^{-3} S cm^{-1} at 293 K to 1.7×10^{-3} S cm^{-1} at 308 K. The plot of ln(σT) versus T^{-1} was linear (Figure 1a inset) and gave an activation energy (E_a) of 0.22 eV for the ionic conductivity. As the humidity was decreased, the σ value drastically decreased from 1.2×10^{-3} S cm^{-1} at 100% RH to 3.2×10^{-8} S cm^{-1} at 8% RH (Figure 1b) while the E_a value increased (e.g., 0.48 eV at 28% RH; Figure S2).

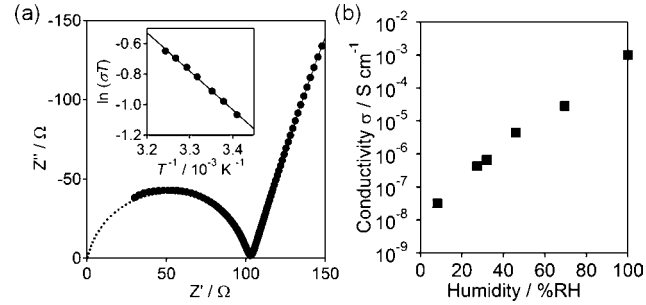

Figure 1. (a) Z' vs Z'' plot of the complex-plane impedance for $Co^{II}[Cr^{III}(CN)_6]_{2/3}\cdot zH_2O$ (**1**) at 100% RH at 293 K. Inset: Plot of ln(σT) vs T^{-1} at 100% RH. (b) Plot of σ vs relative humidity for $Co^{II}[Cr^{III}(CN)_6]_{2/3}\cdot zH_2O$ at 293 K.

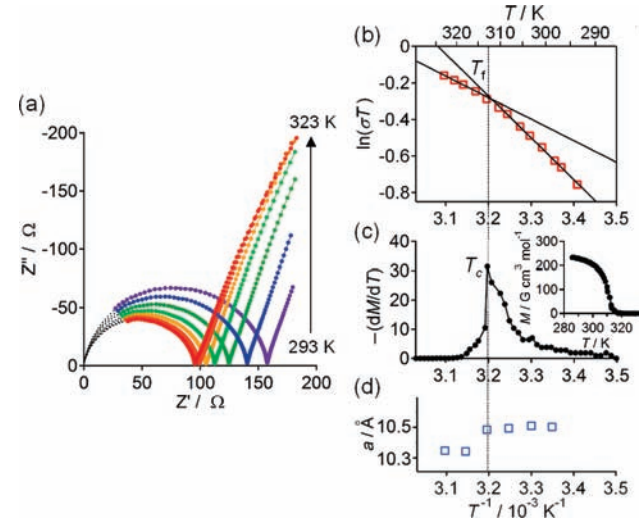

Figure 2. (a) Z' vs Z'' plots for $V^{II}[Cr^{III}(CN)_6]_{2/3}\cdot zH_2O$ at various temperatures. (b) Plot of ln(σT) vs T^{-1} at 100% RH. (c) Plot of the derivative of the magnetization, $-(dM/dT)$, vs T^{-1}. Inset: M vs T plot at 10 Oe. (d) Lattice constant as a function of T^{-1} at 100% RH.

Figure 2a shows plots of Z' versus Z'' for **2** and indicates that σ was 1.6×10^{-3} S cm^{-1} at 293 K and 100% RH. The σ value increased from 1.6×10^{-3} S cm^{-1} at 293 K to 2.6×10^{-3} S cm^{-1} at 323 K as the temperature was increased. However, the slope of the ln(σT) versus T^{-1} plot changed at an intermediate temperature (Figure 2b). The E_a values in the high- and low-temperature regions were 0.10 and 0.19 eV, respectively. The folding point (T_f) of 313

10.1021/ja100385f

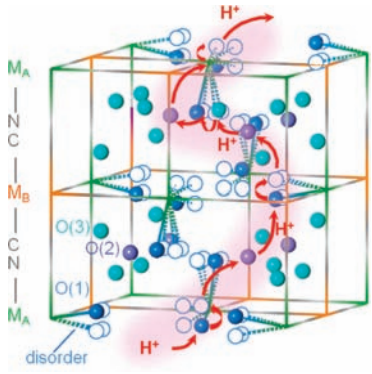

Figure 3. Schematic illustration of the crystal structure of $M_A[M_B(CN)_6]_{2/3}\cdot zH_2O$ and possible pathway of the proton transfer through hydrogen bonds between ligand water and zeolitic water molecules (red arrows). The M_B-CN-M_A framework is drawn as stick lines, and water oxygen atoms are drawn as balls. Green, orange, dark-gray, light-gray, blue, purple, and light-blue colors represent M_A, M_B, C, N, O(1) atoms of ligand water molecules, and O(2) and O(3) atoms of zeolitic water molecules, respectively.

K corresponds to a magnetic phase transition temperature (T_C) in the magnetization versus temperature curve (Figure 2c). Such a T_f point was not observed for **1** or other Prussian blue analogues over the temperature range 293−323 K (Figure S3). In addition, in a V−Cr Prussian blue analogue with a different T_C value, its T_f point corresponded to the T_C value (Figure S4). The temperature dependence of IR spectrum showed changes in the CN stretching and OH stretching peaks around T_C (Figure S5). Furthermore, the temperature dependence of the XRD pattern showed a drastic change in the lattice constant of the fcc structure around T_C (Figure 2d). These results indicate that magnetic ordering affects the ionic conductivity through the variation in the crystal structure.

The σ values of 1.2×10^{-3} S cm^{-1} for **1** and 1.6×10^{-3} S cm^{-1} for **2** are very high, so **1** and **2** can be classified as superionic conductors ($\sigma > 10^{-4}$ S cm^{-1}).[6] These compounds did not contain alkali cation, as determined from the results of elemental analyses, indicating that the ionic conductivity due to the alkali cation was negligible. In addition, the remarkable humidity effect on the ionic conductivity excludes the hopping mechanism due to mixed valency between M_A and M_B. Plots of humidity versus sample weight for **1** showed that the number of H_2O molecules decreased with decreasing humidity. Hence, the following was used to deduce the mechanism of the observed ionic conductivity. In the vacancy sites of $[M_B(CN)_6]^{3-}$, the ligand water molecules coordinate to the M_A ions, and zeolitic water molecules exist (Figure 3). The M_A ion acts as a Lewis acid, and a proton is carried through the 3D hydrogen-bonding network, which is composed of zeolitic water and ligand water molecules (i.e., the proton conductivity is due to the Grotthus mechanism). The increase in the E_a value below T_C may be explained by the expansion of cell volume because such an expansion would inhibit the proton transfer.

Several mechanisms are likely to be involved in the magnetic−ionic conductive interference effect, such as the coupling effect between spin polarization and ionic conductivity and the coupling effect between magnetostriction and ionic conductivity. The former is probably very weak. Thus, it is likely that the latter is predominant. In fact, the temperature dependence of the IR spectrum and XRD pattern of **2** showed drastic changes in OH stretching and CN stretching peaks and lattice constant. It may be that below T_C, magnetic ordering induces magnetostriction, which would slightly distort the M_B-CN-M_A framework. This distortion would affect the 3D hydrogen-bonding network between the ligand water and zeolitic water molecules, altering E_a.

Recently, proton conductivity has been reported in the field of coordination polymers.[7,8] In the present work, Co−Cr and V−Cr Prussian blue analogues exhibited high proton conductivities of 1.2×10^{-3} and 1.6×10^{-3} S cm^{-1}, respectively, at room temperature. The origin of the high proton conduction is explained by a Grotthus mechanism, i.e., proton transfer is mediated by the 3D hydrogen-bonding network of zeolitic water molecules. Furthermore, we have observed an interference effect between magnetic ordering and proton conduction, which is likely due to distortion of the 3D hydrogen-bonding network by magnetostriction below T_C. The observation of such an interference effect may open a new field, so-called *spin-ionics*.

Acknowledgment. We are thankful to JSPS for a Grant-in-Aid for Young Scientists (S), the Global COE Program "Chemistry Innovation" from MEXT, Japan, the Izumi Foundation, and The Asahi Glass Foundation.

Supporting Information Available: Temperature dependence of the IR spectrum and XRD pattern of **2**; impedance measurements of **1** at 28% RH, $Mn[Cr(CN)_6]_{2/3}\cdot zH_2O$ at 40% RH, and $K_{0.12}V_{1.49}[Cr(CN)_6]\cdot 8H_2O\cdot(SO_4)_{0.05}$ at 100% RH. This material is available free of charge via the Internet at http://pubs.acs.org.

References

(1) (a) Verdaguer, M.; Bleuzen, A.; Marvaud, V.; Vaissermann, J.; Seuleiman, M.; Desplanches, C.; Scuiller, A.; Train, C.; Garde, R.; Gelly, G.; Lomenech, C.; Rosenman, I.; Veillet, P.; Cartier, C.; Villain, F. *Coord. Chem. Rev.* **1999**, *192*, 1023. (b) Hashimoto, K.; Ohkoshi, S. *Philos. Trans. R. Soc. London, Ser. A* **1999**, *357*, 2977. (c) Mallah, T.; Marvilliers, A.; Rivière, E. *Philos. Trans. R. Soc. London, Ser. A* **1999**, *357*, 3139.

(2) (a) Mallah, T.; Thiebaut, S.; Verdaguer, M.; Veillet, P. *Science* **1993**, *262*, 1554. (b) Entley, W. R.; Girolami, G. S. *Science* **1995**, *268*, 397. (c) Ferlay, S.; Mallah, T.; Ouahès, R.; Veillet, P.; Verdaguer, M. *Nature* **1995**, *378*, 701. (d) Hatlevik, Ø.; Buschmann, W. E.; Zhang, J.; Manson, J. L.; Miller, J. S. *Adv. Mater.* **1999**, *11*, 914. (e) Holmes, S. M.; Girolami, G. S. *J. Am. Chem. Soc.* **1999**, *121*, 5593. (f) Garde, R.; Villain, F.; Verdaguer, M. *J. Am. Chem. Soc.* **2002**, *124*, 10531. (g) Ohkoshi, S.; Mizuno, M.; Hung, G.-J.; Hashimoto, K. *J. Phys. Chem. B* **2000**, *104*, 9365.

(3) (a) Ohkoshi, S.; Hashimoto, K. *J. Photochem. Photobiol., C* **2001**, *2*, 71. (b) Tokoro, H.; Ohkoshi, S.; Hashimoto, K. *Appl. Phys. Lett.* **2003**, *82*, 1245. (c) Sato, O.; Iyoda, T.; Fujishima, A.; Hashimoto, K. *Science* **1996**, *272*, 704. (d) Pejakovic, D. A.; Manson, J. L.; Miller, J. S.; Epstein, A. J. *Phys. Rev. Lett.* **2000**, *85*, 1994. (e) Bleuzen, A.; Lomenech, C.; Escax, V.; Villain, F.; Varret, F.; Cartier dit Moulin, C.; Verdaguer, M. *J. Am. Chem. Soc.* **2000**, *122*, 6648. (f) Varret, F.; Goujon, A.; Boukheddaden, K.; Noguès, M.; Bleuzen, A.; Verdaguer, M. *Mol. Cryst. Liq. Cryst.* **2002**, *379*, 333.

(4) (a) Ohkoshi, S.; Arai, K.; Sato, Y.; Hashimoto, K. *Nat. Mater.* **2004**, *3*, 857. (b) Yanai, N.; Kaneko, W.; Yoneda, K.; Ohba, M.; Kitagawa, S. *J. Am. Chem. Soc.* **2007**, *129*, 3496.

(5) (a) Coronado, E.; Giménez-López, M. C.; Levchenko, G.; Romero, F. M.; Garcia-Baonza, V.; Milner, A.; Paz-Pasternak, M. *J. Am. Chem. Soc.* **2005**, *127*, 4580. (b) Papanikolaou, D.; Kosaka, W.; Margadonna, S.; Kagi, H.; Ohkoshi, S.; Prassides, K. *J. Phys. Chem. C* **2007**, *111*, 8086. (c) Margadonna, S.; Prassides, K.; Fitch, A. N. *J. Am. Chem. Soc.* **2004**, *126*, 15390. (d) Goodwin, A. L.; Chapman, K. W.; Kepert, C. J. *J. Am. Chem. Soc.* **2005**, *127*, 17980. (e) Kaye, S. S.; Choi, H. J.; Long, J. R. *J. Am. Chem. Soc.* **2008**, *130*, 16921. (f) Ohkoshi, S.; Tokoro, H.; Matsuda, T.; Takahashi, H.; Irie, H.; Hashimoto, K. *Angew. Chem., Int. Ed.* **2007**, *46*, 3238.

(6) (a) Colomban, P.; Novak, A. *J. Mol. Struct.* **1988**, *177*, 277. (b) Colomban, P. *Proton Conductors: Solids, Membranes and Gels—Materials and Devices*; Cambridge University Press: Cambridge, U.K., 1992.

(7) (a) Sadakiyo, M.; Yamada, T.; Kitagawa, H. *J. Am. Chem. Soc.* **2009**, *131*, 9906. (b) Okawa, H.; Shigematsu, A.; Sadakiyo, M.; Miyakawa, T.; Ohba, M.; Kitagawa, H. *J. Am. Chem. Soc.* **2009**, *131*, 13516. (c) Bureekaew, S.; Horike, S.; Higuchi, M.; Mizuno, M.; Kawamura, T.; Tanaka, D.; Yanai, N.; Kitagawa, S. *Nat. Mater.* **2009**, *8*, 831. (d) Hurd, J. A.; Vaidhyanathan, R.; Thangadurai, V.; Ratcliffe, C. I.; Moudrakovski, I. L.; Shimizu, G. K. H. *Nat. Chem.* **2009**, *1*, 705.

(8) Recently, Long and co-workers[9] reported that $K_{1.2}Ru_{3.6}[Ru(CN)_6]_3\cdot 16H_2O$ showed an electrical conductivity of 5.6×10^{-3} S cm^{-1}. This high conductivity was explained by a hopping conduction mechanism through intervalence charge transfer (IVCT), not by proton conductivity. In contrast, our systems do not have intense IVCT bands in the visible and near-IR regions.

(9) Behera, J. N.; D'Alessandro, D. M.; Soheilnia, N.; Long, J. R. *Chem. Mater.* **2009**, *21*, 1922.

JA100385F